Selective Functionalization of Tailored Nanostructures

Winand Slingenbergh,[†] Sanne K. de Boer,[†] Thorben Cordes,[‡] Wesley R. Browne,[§] Ben L. Feringa,[§] Jacob P. Hoogenboom,[⊥] Jeff Th. M. De Hosson,[†] and Willem F. van Dorp[†,*]

[†]Applied Physics, [‡]Molecular Microscopy Research Group & Single-Molecule Biophysics, and [§]Stratingh Institute for Chemistry, Zernike Institute for Advanced Materials, University of Groningen, Nijenborgh 4, 9747 AG Groningen, The Netherlands and [⊥]Department of Imaging Science and Technology, Faculty of Applied Sciences, Delft University of Technology, 2628 CJ Delft, The Netherlands

ABSTRACT

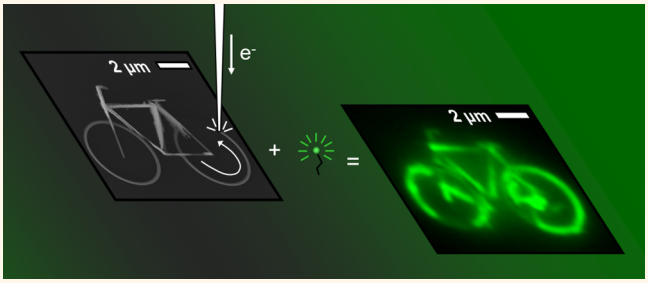

The controlled positioning of nanostructures with active molecular components is of importance throughout nanoscience and nanotechnology. We present a novel three-step method to produce nanostructures that are selectively decorated with functional molecules. We use fluorophores and nanoparticles to functionalize SiO features with defined shapes and with sizes ranging from micrometers to 25 nm. The method is called MACE-ID: molecular assembly controlled by electron-beam-induced deposition. In the first step, SiO nanostructures are written with focused electron-beam-induced deposition, a direct-writing technique. In the second step, the deposits are selectively silanized. In the final step, the silanes are functionalized with fluorescent dyes, polystyrene spheres, or gold nanoparticles. This recipe gives exciting new possibilities for combining the highly accurate control of top-down patterning (e-beam direct writing) with the rich variety of the bottom-up approach (self-assembly), leading to active or responsive surfaces. An important advantage of MACE-ID is that it can be used on substrates that already contain complex features, such as plasmonic structures, nanoantennas, and cavities.

KEYWORDS: selective functionalization · directed self-assembly · local decoration · nanostructures · focused electron-beam-induced deposition

Combining a top-down approach with molecular self-assembly processes can lead to unique and otherwise inaccessible materials for future nanotechnological or biological applications.[1] The key concept in these strategies is the controlled positioning of nanostructures with active molecular components. In nanophotonics, the coupling of optically active molecules to structures like nanoantennas,[2−4] cavities,[5−7] nanoscale waveguides,[8] or mechanical resonators[9] requires the precise positioning of functional molecules.[10] Reporter molecules placed at locations of strong local field enhancement can be used for ultrasensitive detection and analysis.[11] Moreover, nanoscale responsive surfaces can be used to control micro- and nanoscale motion,[12] to measure viscosity on microscopic length scales,[13] and to perform signal processing.[14]

There are a number of techniques to deliver functional molecules to designated positions on a substrate. In many cases, a self-assembled monolayer (SAM) is used. A pattern can be written in the SAM with an electron beam, so that molecular attachment is either locally inhibited (negative writing)[15,16] or enabled (positive writing) after exposure.[17] While the pattern itself can have details on the order of tens of nanometers,[18−20] this local pattern can only be written in a SAM that, inherent to the method, covers the entire substrate. This limits the type of substrate that can be used to those on which SAMs can be formed and makes it difficult to use samples with complex geometries or samples that already contain other functional components. Direct-write techniques such as dip-pen nanolithography[21,22] and single-molecule cut-and-paste[23] can overcome this limitation. They can deliver functional molecules directly, without SAM and even at sub-20 nm resolution. However, these approaches have other limitations, such as the processing speed, compatibility with existing commercial nanofabrication procedures, and the ability to functionalize nonflat surfaces.

We present a novel direct-write nanopatterning technique for the fabrication of nanostructures selectively decorated with functional molecules. We call this technique MACE-ID: molecular assembly controlled by electron-beam-induced deposition. MACE-ID relies on the use of focused

* Address correspondence to w.f.van.dorp@rug.nl.

Received for review August 7, 2012 and accepted September 20, 2012.

Published online September 20, 2012
10.1021/nn303571p

electron-beam-induced deposition (FEBID)[24−26] to deposit SiO nanostructures in the scanning electron microscope. These nanostructures can be selectively functionalized using a silane coupling agent, as we demonstrate with fluorescent molecules, polystyrene (PS) nanospheres, and Au nanoparticles. We show that the recipe works for isolated SiO features with arbitrary shapes and sizes in the range of micrometers down to 25 nm. A major advantage of this approach is that SiO is a well-characterized material for which many functionalization strategies are available. In addition, SiO is optically inactive and transparent. Extension to other deposits such as Au[27] or Pt[28] is possible.

RESULTS AND DISCUSSION

The MACE-ID technique is illustrated in Figure 1. First, we direct-write a SiO nanostructure on the substrate using focused electron-beam-induced deposition. The precursor gas is 2,4,6,8,10-pentamethylcyclopentasiloxane, and the deposits consist of $Si_1O_{1.1}C_{0.06}$ (referred to hereafter as SiO).[29] After direct writing, we silanize the deposit with a coupling agent (Figure 1b), which binds to hydroxyl groups at the surface of the deposit. We use the silanes (3-aminopropyl)triethoxysilane (APTES) or (3-aminopropyl)-dimethylethoxysilane (APDMES). As discussed below, the difference between these two is that APTES is a trifunctional silane and APDMES is monofunctional. The latter allows for an easier monolayer coverage of the deposit. The silanization is performed by submerging the substrate in a solution of the coupling agent in anhydrous toluene. The functional entity, either a molecule or a nanoparticle, is then covalently grafted onto the deposit *via* the silane coupling agent. The 30 nm wide SiO nanodots that are written on a Si wafer (Figure 1d) and the three-dimensional nanotrees around a small house (Figure 1e) are examples of the structures that can be made with FEBID. The nanotrees are branched SiO pillars, created with a point exposure (on the order of seconds) with the focused e-beam.[29] The nanohouse is made by scanning the e-beam in a series of overlaid rectangles, creating the roof by writing smaller rectangles on the existing base.

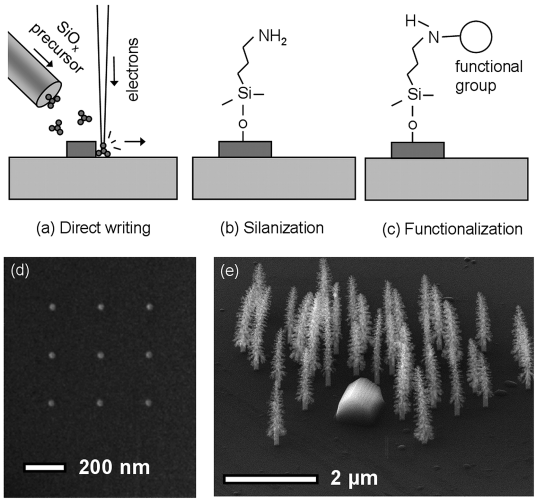

Figure 1. Illustration of the MACE-ID technique with some examples of electron-beam-induced deposition. (a) Nanostructure deposited by exposing a SiO precursor gas to a focused beam of electrons. (b) Silane coupling agent grafted onto the nanostructure. (c) Functional group, such as a fluorophore or a nanoparticle, covalently linked to the nanostructure. (d,e) Electron microscope images of SiO nanostructures written on a Si wafer with FEBID: (d) 30 nm wide dots and (e) three-dimensional structures that can be described as nanotrees around a house-shaped object.

In Figure 2, two fluorescent SiO structures prepared using MACE-ID are shown. Figure 2a shows a SiO bicycle pattern, written with FEBID and imaged using the scanning electron microscope (SEM). Following the procedure in Figure 1a−c, the bicycle pattern is silanized with APTES and functionalized with the fluorescent dye fluorescein isothiocyanate (FITC). When excited at 465 nm, the FITC fluorescence is observed by wide-field microscopy (Figure 2b). The SiO bicycle is functionalized, although not perfectly. Some features (such as the front wheel) are not evenly fluorescent, while extra features appear in the rear wheel. We attribute this to the rinsing and cleaning procedure that is not yet optimized. We discuss this in further detail at the end of this section. In Figure 2c, two arrays consisting of 100 × 100 nm SiO squares are shown, also functionalized with FITC.

Increasing the surface concentration of hydroxyl groups prior to silanization (by exposure to an oxygen plasma or piranha solution) leads to an increase in fluorescence intensity under otherwise similar coating conditions. We have verified that the deposits are fluorescent only when they are functionalized with a fluorophore. If the deposit is silanized with APTES or

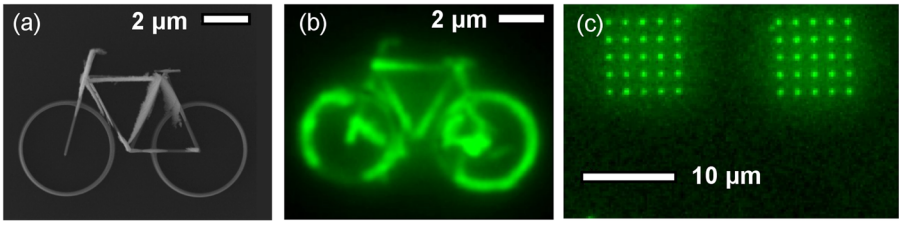

Figure 2. Fluorescent nanostructures fabricated with MACE-ID, written on Si. (a) SEM image of a nanoscale SiO bicycle after FEBID and (b) optical image after silanization with APTES and grafting of the fluorescent dye FITC. (c) Two arrays of FITC fluorescent nanodots observed in the optical microscope. The lateral size of each fluorescent dot is 100 × 100 nm.

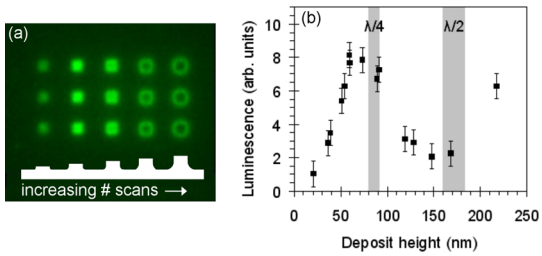

Figure 3. Dependence of the fluorescence intensity on the deposit height on a silicon substrate. (a) FITC fluorescence intensity for nanostructures of, from left to right, increasing height. (b) Fluorescence intensity as function of the deposit height. If we assume a refractive index of 1.4−1.6 for the deposit and a wavelength of 512 nm for the emitted light, the minimum in fluorescence intensity coincides with a deposit height of approximately $\lambda/2$. This indicates destructive interference between the direct electromagnetic wave at the upper surface of the deposit with the wave back-reflected from the substrate.

APDMES and not exposed to FITC, fluorescence is not observed (see the Supporting Information for further details).

Prolonged electron beam exposure or an increase of electron dose during SiO deposition increases the deposit height. Figure 3a shows a sequence of 1×1 μm FITC-functionalized SiO squares written with MACE-ID on a Si substrate, of which the deposit height increases left to right as indicated. We observe a clear dependence of fluorescence intensity on the height of the deposit. We ascribe this to the modified optical mode density due to the presence of the high refractive index Si substrate. Constructive and destructive interference of the EM radiation at the SiO−air interface with the wave back-reflected from the underlying Si−SiO interface causes a modulation in fluorescence intensity as a function of the distance from the Si substrate. It should be noted that upon close inspection of Figure 3a it can be seen that, in the second and third column from the left, the intensity at the edge is weaker than in the center of the square, while this is reversed for the two rightmost columns. This is caused by the columns not having a perfect top-hat profile but having slight "tails". In the rightmost columns of Figure 3a, the tails have sufficient height for constructive interference, while the centers of the squares are higher so that deconstructive interference occurs.

A measurement of luminescence intensity supports this hypothesis for deposit heights up to 200 nm. In Figure 3b, the fluorescence intensity is plotted as function of deposit height and the modulation in intensity is observed. Consistent with thin film interference, the refractive index of the material and the wavelength of the light determine height at which constructive interference (height equal to $\lambda/4$) and deconstructive interference (height equal to $\lambda/2$) occur. Assuming a refractive index of the SiO deposit of $n = 1.4-1.6$ and a free-space emission wavelength of 512 nm for FITC gives an effective wavelength of 320−365 nm in the deposit. From Figure 3b, we observe that the maximum and minimum in intensity are in good agreement with $\lambda_{eff}/4$ and $\lambda_{eff}/2$, respectively. The observed slight deviation may be ascribed to penetration of the electromagnetic field in the Si substrate and/or an underestimation of the SiO's refractive index. It is known that the refractive index of glass varies depending on composition and structure. If we would solely consider the refractive index of SiO, based on the data presented in Figure 3b, we find the best fit for $n = 1.7$.

We cannot exclude the possibility that the luminescence is partially affected by the porosity of the deposit. If the SiO is porous, the internal surface area increases with increasing deposit height. This would also lead to an increase in intensity with increasing deposit height. However, we conclude from the modulation in fluorescence intensity that changes in the optical mode density are dominant.

Other than the electron dose, which is a determining factor for the height of the deposits, the scan conditions do not influence the final fluorescence intensity. If the beam current is increased while the total electron dose is kept constant, we do not observe any significant change in fluorescence. See the Supporting Information for more details.

In the preceding paragraphs, we have demonstrated that SiO deposits created with electron beam exposure can be successfully functionalized with a fluorescent dye (MACE-ID). We note that the functionalization reaction described above will occur not soley on the SiO deposit but also on the native oxide layer of the Si substrate. In the following experiments, we first use functionalization on the Si native oxide layer to fine-tune the conditions for MACE-ID and then apply the scheme to selectively functionalize nanostructures at monolayer coverage.

The silanization of SiO is investigated further by functionalization with carboxyl-actived polystyrene (PS) spheres and Au nanoparticles.[30] These particles serve as markers that can be easily inspected with the SEM. In this way, we avoid complications due to low optical signals at low dye coverage and quenching or interference effects close to a substrate, as encountered in the images in Figure 3. Figure 4 shows SEM images of silicon wafers, of which the native oxide is functionalized with carboxyl-coated PS spheres and Au nanoparticles. Again, we have confirmed that functionalization does not occur in the absence of APTES (Figure 4c; see also Supporting Information). The experiments with PS spheres show that it is crucial to keep the sample wet during the functionalization procedure to prevent unselective decoration and the formation of agglomerates on the surface. Reproducible results are only obtained when the sample stays submerged in liquid during the transfer from solution to solution. A specially designed sample holder is described in detail in the Methods section.

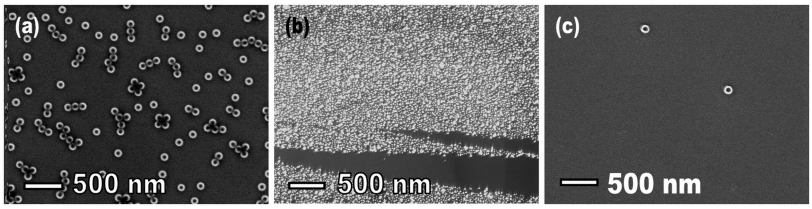

Figure 4. Functionalization of the native oxide layer on an APTES-coated Si wafer is inspected with the SEM using (a) polystyrene spheres and (b) gold nanoparticles as label. (c) Without APTES, there is no functionalization of the Si wafer (apart from polystyrene spheres that remain after an incomplete washing step).

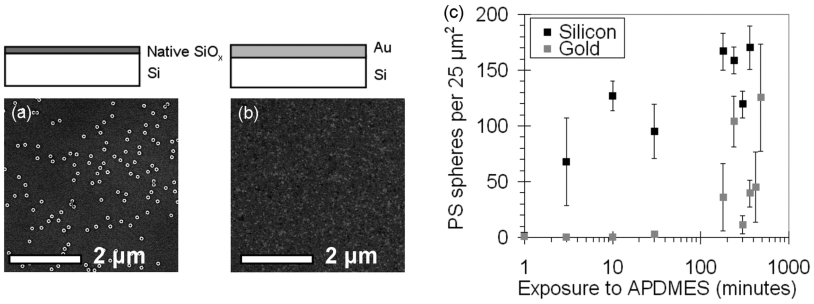

Figure 5. Selective functionalization of SiO_x with APDMES as coupling agent, determined with the SEM. (a) PS spheres bind to APDMES-coated native oxide layer on a Si wafer. (b) Particle attachment is not observed on a Au-coated Si wafer treated with APDMES. (c) Au *vs* SiO_x selectivity is maintained for exposure times up 30 min in the APDMES solution. Similar results were obtained when using coating with diamond-like carbon instead of Au.

Experiments with PS spheres and Au nanoparticles show that the functionalization process is difficult to control when using APTES as a coupling agent. We estimate a monolayer coverage from the concentration of APTES in anhydrous toluene (for a time in solution of 30 min) at which the surface concentration of PS spheres, inspected in the SEM, saturates. A monolayer coverage on the native oxide of a silicon wafer is observed at concentrations of 1−2.5 μM, which is low compared to concentrations reported in literature.[31] However, the reproducibility of the surface coverage is poor, and more importantly, the silanization is not always selective. For instance, if we write a SiO deposit on a Au-coated wafer, PS spheres are found on the Au as well as on the SiO. We speculate that the trifunctional APTES polymerizes in solution due to hydrolysis. If polymerized APTES settles on the surface from the solution (whether on SiO or on Au), it forms multilayers that adhere unselectively to the surface. This multilayer can subsequently be functionalized. As a result, the silanization is difficult to control, despite the use of anhydrous toluene.

To increase our control over the selectivity, we replace APTES with (3-aminopropyl)dimethylethoxysilane in anhydrous toluene. APDMES is a monofunctional aminosilane, for which we expect that dimerization in solution does not have further effects. To verify the selectivity, we compare the silanization between a Au-coated wafer and the native oxide of a silicon wafer. After silanization, the samples are functionalized with PS spheres. The results are shown in Figure 5, where the surface concentration (PS spheres per 25 μm^2) is plotted as function of the immersion time in the APDMES solution. It is observed that for exposures up to 30 min PS spheres are only found on the native oxide and not on the Au surfaces. Therefore, in this regime, the silanization is selective. It is also observed that at longer exposure times (>100 min) PS spheres are observed on the Au surface, as well. We speculate that this is due to impurities in the APDMES (purity is 97%). If these impurities are multifunctional aminosilanes (such as APTES), they can self-assemble a-selectively on the surface.

Additional experiments indicate that a similar selectivity as for Au-coated Si can be obtained on diamond-like carbon (DLC)-coated silicon wafers for exposure times shorter than 30 min (data not shown).

Now that we have identified the regime for selective silanization of the native oxide of a Si wafer in Figure 5c, we apply these conditions, with APDMES, to MACE-ID. Figure 6a shows SiO lines written on a Au-coated wafer. Figure 6b shows one of the lines at a higher magnification. The thin SiO is (partially) transparent to the electrons, but the line scan shows a width of 25 nm. After silanization with APDMES for 10 min, the SiO lines are functionalized with the fluorophore ATTO655. When illuminated at 643 nm and observed by optical microscopy, the luminescence is clearly distinguished.

With MACE-ID, the resolution of the functionalization can be expected to go beyond the 25 nm that we demonstrate here. We expect that 10 nm SiO features can be written with the setup currently used for the deposition. FEBID patterns with details smaller than 5 nm have been reported,[32−34] and the state-of-the-art for writing deposits on a Si wafer is 3 nm.[35]

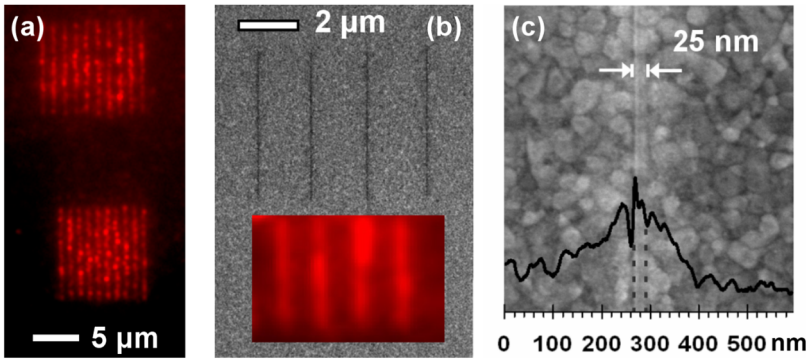

Figure 6. MACE-ID of SiO lines on Au. (a) Optical image of parallel lines after functionalization with APDMES and the fluorescent dye ATTO655. The intensity gradient from top to bottom is due to a slight misalignment of the microscope. (b) SEM micrograph of SiO lines on Au. The inset shows the optical fluorescence image of the same lines after functionalization. (b) From the line scan in the SEM micrograph, it is observed that the line width is 25 nm.

If the deposition is performed on an electron-transparent membrane and in a transmission electron microscope, sub-nanometer resolutions are possible.[36] It is currently unknown how smooth SiO lines are if they are less than 10 nm wide or how the functional molecules are distributed on the surface of such lines. This is the topic of current experiments.

We observe that the control over the surface functionalization with MACE-ID is not fully optimized yet. In Figure 2b, fluorescent features are visible (for instance, in the wheels of the bike) that were not written with the e-beam. Also, there are intensity variations along the patterns in Figure 6a,b. This is due to impurities introduced onto the sample surface, variations in the surface concentration of fluorophores, and sonication used to clean the samples in the experiments as presently described. Sonication is known to damage graphene oxide[37] and remove fluorophores from the surface.[38] We have observed in the SEM that it can cause the FEBID SiO (such as lines and parts of the bike in Figure 2b) to detach from the surface and that it removes covalently bound PS spheres from the surface. The less-than-perfect pattern transfer is also caused by the fact that the samples are allowed to dry between the preparation steps. This is a likely source for impurities because the experiments are done in a standard fume hood and not in a clean room. We are currently working on improving the cleaning procedure and eliminating the need for sonication.

CONCLUSIONS

In conclusion, our work shows that FEBID allows the selective functionalization of locally deposited SiO with organic compounds down to pattern sizes as small as 25 nm. The SiO is silanized following the writing with the e-beam, after which it is ready to be decorated with functional molecules. Patterns of any particular shape, two- or three-dimensional, are written on the surface directly. The use of a resist layer or self-assembling monolayer that covers the entire sample is not necessary. We demonstrate the functionalization with fluorophores, polystyrene spheres, and gold nanoparticles. Selective functionalization is possible with the monofunctional silane APDMES. In contrast, the trifunctional silane APTES leads to poor reproducibility and an unselective coverage of the sample, which we contribute to hydrolysis in solution. The intensity of the light emitted from fluorophores on the SiO depends on the height of the deposits. Measurements indicate that this height effect is consistent with thin film interference, where the EM radiation emitted by the fluorophore negatively interferes with that back-reflected from the underlying Si−SiO interface.

The process described provides exciting new opportunities for combining the highly accurate control of top-down patterning (e-beam direct writing) with the rich variety of the bottom-up approach (self-assembly) leading to responsive surfaces. It opens the possibility of functionalization with a large variety of molecules, where multiple functionalities can be incorporated by repeating the procedure or depositing different materials. A key advantage of MACE-ID is that it can be used on substrates that already contain complex features, such as plasmonic structures, nanoantennas, and cavities. MACE-ID nanoassemblies can, for instance, be used to couple functional molecules to plasmonic structures.

METHODS

Direct Writing. The focused electron-beam-induced deposition is performed on a Tescan Lyra dual beam system, equipped with a field emission electron gun, which is operated at 10−30 keV. The beam currents are measured with a Faraday cup and vary between 80 pA and 2 nA. The minimum spot size is around 3.5 nm. The SiO precursor is 2,4,6,8,10-pentamethylcyclopentasiloxane, introduced into the vacuum chamber through a multigas injection system positioned close to the sample. Prior to deposition, the sample chamber is plasma cleaned for at least 12 h using an XEI Scientific Evactron 25 De-Contaminator. During the cleaning, the sample is placed in the sample chamber.

The background pressure is better than 5×10^{-6} mbar, and the chamber pressure during writing is around 4×10^{-5} mbar. The local precursor pressure at the sample is unknown. The pattern is written using TESCANs proprietary patterning software without the use of a beam blanker. We do not observe an influence of the beam current on the functionalization of the SiO.

Samples. Patterns are written on a doped Si wafer with a native oxide or on a silicon wafer coated with 100 nm polycrystalline Au (Sigma-Aldrich). FEBID SiO has also been written on a Si wafer coated with 750 nm diamond-like carbon, applied by physical vapor deposition.

Sample Preparation. The SiO deposited with FEBID is inherently hydroxyl-terminated. The surface concentration of hydroxyl groups can be enhanced by exposing the sample to piranha solution (a 7:3 mixture of H_2SO_4 and H_2O_2) or an oxygen plasma. After using a piranha solution, the samples are rinsed with Milli-Q water and ethanol. The final step is drying under a stream of nitrogen.

Dry samples are handled with clean tweezers. Treatments in liquid are done in new 20 mL scintillation vials as received. We have observed that the manipulation of wet samples with tweezers in glass vials and the transfer of the sample between solutions is a cause for damage. Our experiments with the PS spheres show that especially the (unintended) drying of the sample during the transfer through air with a pair of tweezers from vial to vial causes unselective functionalization and the presence of dirt on the sample. We use a dedicated sample holder during the functionalization to prevent this, which is a Teflon disk with a cavity of about 1 mm deep. The sample lies flat in the cavity, and in turn, the Tefon disk lies flat on the bottom of the vial in the solution. A vertical rod is attached to the Teflon disk to manipulate it. The cavity is shallow enough to allow the sample to react with the solution. At the same time, the cavity causes the sample to stay submerged in about 0.2 mL of liquid during the transfer from vial to vial. During rinsing in a solvent, the sample is lifted from the cavity with a pair of tweezers to make sure that the cavity and underside of the sample are cleaned properly.

Silanization. The (3-aminopropyl)triethoxysilane (APTES, CAS 919-30-2, Sigma-Aldrich) is dissolved in anhydrous toluene and used in concentrations of 0.05 to 0.0005 mM. The (3-aminopropyl)dimethylethoxysilane (APDMES, CAS 18306-79-1, Acros-Organics) is of 97% purity according to the supplier. The APDMES is dissolved in anhydrous toluene at 1% (v/v) under a nitrogen atmosphere. Silanization is done at a solution temperature of 65−70 °C for 1 min to 20 h. After silanization, the samples are rinsed and cleaned in an ultrasonic bath.

Functionalization. The fluorescein isothiocyanate (FITC, CAS 3326-32-7, Acros-Organics) is dissolved in ethanol in a concentration of 0.01 mM. Samples are submersed for 15 min at room temperature for functionalization.

The ATTO655 (CAS 485815-43-8, ATTO-TEC GmbH) is dissolved in Milli-Q water in a concentration of 1 μM with a $NaHCO_3$ buffer, giving the solution a pH of 8.2. The samples are submersed at room temperature for 1 min for functionalization.

The polystyrene (PS) spheres (PC02N/8748, 1.06 g/cm^3, Bangs Laboratories) have a diameter of 120 nm diameter and are carboxyl-modified. Grafting onto the deposit or Si wafer is done with EDC (CAS 1892-57-5) and NHS (CAS 6066-82-6) from Fluka. The silanized sample is placed in a solution of 0.5 mL of EDC/NHS and 7 mL of PS in water (dilution to 10% of the original PS concentration) for 15 min at room temperature. Mild stirring of the suspension is necessary to obtain a sufficient and reproducible coverage of PS spheres on the surface.

Colloidal Au nanoparticles are produced *via* the Frens method[39] and have an average diameter of about 15 nm. Samples are placed into the suspension of Au nanoparticles for 1 h at room temperature.

In all cases, samples are rinsed at least three times in ethanol or Milli-Q water and sonicated for 10 s, after which they are dried in a stream of nitrogen.

Microscopy. High-resolution imaging is done with electron energies between 5 and 30 keV with Philips XL30, XL30S, or XL30 ESEM scanning electron microscopes, all equipped with a field emission source. The deposit height is measured in air with a Digital Instruments Nanoscope IIIa atomic force microscope, operated in tapping mode. The Veeco n-doped uncoated Si cantilever has a force constant of 20−80 N/m and a characteristic frequency of 300−366 kHz. We have not measured the tip diameter.

Fluorescence Imaging. Epifluorescence and wide-field microscopy of FITC-functionalized samples is carried out using a CoolLED precisExcite High-power LED (465 nm) illumination attached to a Nikon TE Eclipse microscope. An Andor iXON DU897 emCCD camera is used for image acquisition, and Semrock filters are mounted in a Nikon filter cube (exciter wavelength 482 (±18) nm, emitter wavelength 525 (±45) nm, dichroic wavelength 501−900 nm). A Nikon 60× oil and a Nikon 100× oil objective are used with a numerical aperture of 1.49 and a working distance of 0.13 mm.

Epifluorescence and wide-field microscopy of samples functionalized with ATTO655 are imaged with a custom-made microscope based on an Olympus X71 body. A 643 nm solid-state Coherent Cube 640-100C laser is used for fluorophore excitation in combination with a Hamamatsu emCCD camera for imaging. Band-pass ET 700/75 filters and a 100× Olympus objective with a numerical aperture of 1.49 are used.

Conflict of Interest: The authors declare no competing financial interest.

Acknowledgment. This work has been supported by VENI Grant No. 10684 through the Foundation of Technical Sciences (STW-Utrecht).

Supporting Information Available: More experimental details and supplementary data. This material is available free of charge *via* the Internet at http://pubs.acs.org.

REFERENCES AND NOTES

1. Van der Molen, S. J.; Liao, J. H.; Kudernac, T.; Agustsson, J. S.; Bernard, L.; Calame, M.; Van Wees, B. J.; Feringa, B. L.; Schonenberger, C. Light-Controlled Conductance Switching of Ordered Metal−Molecule−Metal Devices. *Nano Lett.* **2009**, *9*, 76–80.
2. Curto, A. G.; Volpe, G.; Taminiau, T. H.; Kreuzer, M. P.; Quidant, R.; Van Hulst, N. F. Unidirectional Emission of a Quantum Dot Coupled to a Nanoantenna. *Science* **2010**, *329*, 930–933.
3. Novotny, L.; Van Hulst, N. F. Antennas for Light. *Nat. Photonics* **2011**, *5*, 83–90.
4. Biagioni, P.; Huang, J. S.; Hecht, B. Nanoantennas for Visible and Infrared Radiation. *Rep. Prog. Phys.* **2012**, *75*, 024402.
5. Englund, D.; Fattal, D.; Waks, E.; Solomon, G.; Zhang, B.; Nakaoka, T.; Arakawa, Y.; Yamamoto, Y.; Vuckovic, J. Controlling the Spontaneous Emission Rate of Single Quantum Dots in a Two-Dimensional Photonic Crystal. *Phys. Rev. Lett.* **2005**, *95*, 013904.
6. Noda, S.; Fujita, M.; Asano, T. Spontaneous-Emission Control by Photonic Crystals and Nanocavities. *Nat. Photonics* **2007**, *1*, 449–458.
7. Hoogenboom, J. P.; Sanchez-Mosteiro, G.; Colas des Francs, G.; Heinis, D.; Legay, G.; Dereux, A.; Van Hulst, N. F. The Single-Molecule Probe: Vectorial Mapping of Photonic Mode Density in a Metal Mirror Cavity. *Nano Lett.* **2009**, *9*, 1189–1195.
8. Chen, Y.; Wubs, M.; Mørk, J.; Koenderink, A. F. Coherent Single-Photon Absorption by Single Emitters Coupled to One-Dimensional Nanophotonic Waveguides. *New J. Phys.* **2011**, *13*, 103010.
9. Arcizet, O.; Jacques, V.; Siria, A.; Poncharal, P.; Vincent, P.; Seidelin, S. A Single NV Defect Coupled to a Nanomechanical Oscillator. *Nat. Phys.* **2011**, *7*, 879–883.
10. Cordes, T.; Strackharn, M.; Stahl, S. W.; Summerer, W.; Steinhauer, C.; Forthmann, C.; Puchner, E. M.; Vogelsang, J.; Gaub, H. E.; Tinnefeld, P. Resolving Single-Molecule Assembled Patterns with Superresolution Blink-Microscopy. *Nano Lett.* **2010**, *10*, 645–651.
11. Fang, Y.; Seong, N. H.; Dlott, D. D. Measurement of the Distribution of Site Enhancements in Surface-Enhanced Raman Scattering. *Science* **2008**, *321*, 388–392.

12. Eelkema, R.; Pollard, M. M.; Vicario, J.; Katsonis, N.; Serrano Ramon, B.; Bastiaansen, C. W. M.; Broer, D. J.; Feringa, B. L. Molecular Machines: Nanomotor Rotates Microscale Objects. *Nature* **2006**, *440*, 163.
13. Haidekker, M. A.; Theodorakis, E. A. Molecular Rotors—Fluorescent Biosensors for Viscosity and Flow. *Org. Biomol. Chem.* **2007**, *5*, 1669–1678.
14. Winston, E. B.; Lowell, P. J.; Vacek, J.; Chocholousova, J.; Michl, J.; Price, J. C. Dipolar Molecular Rotors in the Metal−Organic Framework Crystal IRMOF-2. *Phys. Chem. Chem. Phys.* **2008**, *10*, 5188–5191.
15. Harnett, C. K.; Satyalakshmi, K. M.; Craighead, H. G. Low-Energy Electron-Beam Patterning of Amine-Functionalized Self-Assembled Monolayers. *Appl. Phys. Lett.* **2000**, *76*, 2466–2468.
16. Rundqvist, J; Hoh, J. H.; Haviland, D. B. Directed Immobilization of Protein-Coated Nanospheres to Nanometer-Scale Patterns Fabricated by Electron Beam Lithography of Poly(ethylene glycol) Self-Assembled Monolayers. *Langmuir* **2006**, *22*, 5100–5107.
17. Schlapak, R.; Danzberger, J.; Armitage, D.; Morgan, D.; Ebner, A.; Hinterdorfer, P.; Pollheimer, P.; Gruber, J.; Schäffler, F.; Howorka, S. Painting with Biomolecules at the Nanoscale: Biofunctionalization with Tunable Surface Densities. *Nano Lett.* **2012**, *12*, 1983–1989.
18. Gölzhäuser, A.; Eck, W.; Geyer, W.; Stadler, V.; Weimann, T.; Hinze, P.; Grunze, M. Chemical Nanolithography with Electron Beams. *Adv. Mater.* **2001**, *13*, 803–806.
19. Miyake, T.; Tanii, T.; Kato, K.; Zako, T.; Funatsu, T.; Ohdomari, I. Selectivity Improvement in Protein Nanopatterning with a Hydroxy-Terminated Self-Assembled Monolayer Template. *Nanotechnology* **2007**, *18*, 305304.
20. Xu, S.; Miller, S.; Laibinis, P. E.; Liu, G. Y. Fabrication of Nanometer Scale Patterns within Self-Assembled Monolayers by Nanografting. *Langmuir* **1999**, *15*, 7244–7251.
21. Piner, R. D.; Zhu, J.; Xu, F.; Hong, S.; Mirkin, C. A. "Dip-Pen" Nanolithography. *Science* **1999**, *283*, 661–663.
22. Hong, S.; Zhu, J.; Mirkin, C. A. Multiple Ink Nanolithography: Toward a Multiple-Pen Nano-Plotter. *Science* **1999**, *286*, 523–525.
23. Kufer, S. K.; Puchner, E. M.; Gumpp, H.; Liedl, T.; Gaub, H. E. Single-Molecule Cut-and-Paste Surface Assembly. *Science* **2008**, *319*, 594–596.
24. Utke, I.; Hoffman, P.; Melngailis, J. Gas-Assisted Focused Electron Beam and Ion Beam Processing and Fabrication. *J. Vac. Sci. Technol., B* **2008**, *26*, 1197–1276.
25. Botman, A.; Mulders, J. J. L.; Hagen, C. W. Creating Pure Nanostructures from Electron-Beam-Induced Deposition Using Purification Techniques: A Technology Perspective. *Nanotechnology* **2009**, *20*, 372001.
26. Van Dorp, W. F.; Hagen, C. W. A Critical Literature Review of Focused Electron Beam Induced Deposition. *J. Appl. Phys.* **2008**, *104*, 081301.
27. Utke, I.; Hoffmann, P.; Dwir, B.; Leifer, K.; Kapon, E.; Doppelt, P. Focused Electron Beam Induced Deposition of Gold. *J. Vac. Sci. Technol., B* **2000**, *18*, 3168–3171.
28. Botman, A.; Hagen, C. W.; Li, J.; Thiel, B. L.; Dunn, K. A.; Mulders, J. J. L.; Randolph, S.; Toth, M. Electron Postgrowth Irradiation of Platinum-Containing Nanostructures Grown by Electron-Beam-Induced Deposition from $Pt(PF_3)_4$. *J. Vac. Sci. Technol., B* **2009**, *27*, 2759–2763.
29. De Boer, S. K.; Van Dorp, W. F.; De Hosson, J. T. M. Charging Effects During Focused Electron Beam Induced Deposition of Silicon Oxide. *J. Vac. Sci. Technol., B* **2011**, *29*, 06FD01.
30. Leff, D. V.; Brandt, L.; Heath, J. R. Synthesis and Characterization of Hydrophobic, Organically-Soluble Gold Nanocrystals Functionalized with Primary Amines. *Langmuir* **1996**, *12*, 4723–4730.
31. Schwartz, D. K. Mechanisms and Kinetics of Self-Assembled Monolayer Formation. *Annu. Rev. Phys. Chem.* **2001**, *52*, 107–137.
32. Crozier, P. A.; Tolle, J.; Kouvetakis, J.; Ritter, C. Synthesis of Uniform GaN Quantum Dot Arrays *via* Electron Nanolithography of D_2GaN_3. *Appl. Phys. Lett.* **2004**, *84*, 3441–3443.
33. Mitsuishi, K.; Shimojo, M.; Han, M.; Furuya, K. Electron-Beam-Induced Deposition Using a Subnanometer-Sized Probe of High-Energy Electrons. *Appl. Phys. Lett.* **2003**, *83*, 2064–2066.
34. Jiang, H.; Borca, C. N.; Xu, B.; Robertson, B. W. Fabrication of 2- and 3-Dimensional Nanostructures. *Int. J. Mod. Phys. B* **2001**, *15*, 3207–3213.
35. Van Oven, J. C.; Berwald, F.; Berggren, K. K.; Kruit, P.; Hagen, C. W. Electron-Beam-Induced Deposition of 3-nm-Half-Pitch Patterns on Bulk Si. *J. Vac. Sci. Technol., B* **2011**, *29*, 06F305.
36. Van Dorp, W. F.; Zhang, X.; Feringa, B. L.; Wagner, J. B.; Hansen, T. W.; De Hosson, J. Th. M. Nanometer-Scale Lithography on Microscopically Clean Graphene. *Nanotechnology* **2011**, *22*, 505303.
37. Dreyer, D. R.; Park, S.; Bielawski, C. W.; Ruoff, R. S. The Chemistry of Graphene Oxide. *Chem. Soc. Rev.* **2010**, *39*, 228–240.
38. Aimon, S.; Manzi, J.; Schmidt, D.; Poveda Larrosa, J. A.; Bassereau, P.; Toombes, G. E. Functional Reconstitution of a Voltage-Gated Potassium Channel in Giant Unilamellar Vesicles. *PLoS ONE* **2011**, *6*, e25529.
39. Frens, G. Controlled Nucleation for the Regulation of the Particle Size in Monodisperse Gold Suspensions. *Nature* **1973**, *241*, 20–22.